Geological record of marine tsunami-backwash: the role of the hydraulic jump

Slootman, Arnoud; Simpson, Guy; Castelltort, Sébastien; de Boer, Poppe L.

The Depositional Record
The journal of the International Association of Sedimentologists
Open Access

ORIGINAL RESEARCH ARTICLE

Geological record of marine tsunami backwash: The role of the hydraulic jump

ARNOUD SLOOTMAN*,†, GUY SIMPSON†, SÉBASTIEN CASTELLTORT† and POPPE L. DE BOER‡

*College of Petroleum Engineering & Geosciences, King Fahd University of Petroleum and Minerals, Dhahran 31261, Saudi Arabia (E-mail: arnoudslootman@gmail.com)
†Department of Earth Sciences, University of Geneva, Rue des Maraîchers 13, Geneva 1205, Switzerland
‡Faculty of Geosciences, Utrecht University, PO Box 80.115, 3508 TC, Utrecht, the Netherlands

Keywords
Antidune, backset-bedding, Froude supercritical, hydraulic jump, tsunami backwash.

Manuscript received: 23 March 2017; Accepted: 12 December 2017

doi: 10.1002/dep2.38

ABSTRACT

Tsunamis are marked by distinct phases of uprush during coastal inundation and backwash when tsunami water recedes. Especially in the case of a steep coastal profile, the return flow may operate in a Froude-supercritical regime, eroding the flooded area and transporting large volumes of sediment seawards. Important sediment accumulation occurs when the supercritical flow goes through a hydraulic jump where it becomes subcritical upon deceleration. An inferred example in coarse-grained, mixed carbonates from the Lower Pleistocene on Rhodes (Greece) is described, with offshore bars up to 10 m long with scour-and-fill structures and steep antidune stratification. In finer-grained sandy depositional systems such structures may be much longer, up to hundreds of metres. It is suggested here that, analogous to some turbidite beds, the apparent lack of structures or the presence of faint stratification that is common for graded sand layers within marine tsunamiites may in fact consist of extremely low-angle, landward-dipping backset-strata that formed under a landward-migrating hydraulic jump during the basinward retreat of tsunami water. Numerical simulations that focus on the internal stratification of backwash-generated offshore bars support this hypothesis. The recognition of such deposits in the sedimentary record enlarges the toolbox for assessing the past frequency of tsunamis in coastal areas.

INTRODUCTION

Tsunamis cause great natural disasters, killing thousands of people (Morgan *et al.*, 2006; Marano *et al.*, 2010) and incurring extreme property damage (Fraser *et al.*, 2013; Suppasri *et al.*, 2013). Recent occurrences (e.g. Papua New Guinea, 1998; Sumatra, 2004; Chile, 2010; Japan, 2011) have fuelled vigorous research (>500 peer-reviewed articles in the period 2006 to 2012, see Shanmugam, 2012), much of which aimed at risk mitigation of coastal communities and infrastructure (Tsutsumi *et al.*, 2000; Eisner, 2005; Lavigne *et al.*, 2009; Teh *et al.*, 2009; Joseph, 2011; Thuy *et al.*, 2012) and the understanding of tsunami intensity and recurrence intervals (Minoura *et al.*, 2001; Papadopoulos & Fokaefs, 2005; Monecke *et al.*, 2008; Prendergast *et al.*, 2012; Sørensen *et al.*, 2012; Puga-Bernabéu *et al.*, 2013). The offshore geological record is a potentially rich archive of tsunami impacts (Einsele *et al.*, 1996; Weiss & Bahlburg, 2006; Dawson & Stewart, 2008; Slootman *et al.*, 2016) over time scales much longer than those obtained from historical records (Scheffers & Kelletat, 2003; Papadopoulos & Fokaefs, 2005; Dominey-Howes, 2007; Soloviev *et al.*, 2013). The potential of the geological record in assessing tsunami hazard and risk mitigation relies on the correct identification of associated processes and deposits (Clague *et al.*, 2000; Dominey-Howes, 2002; Jaffe & Gelfenbaum, 2002; Dominey-Howes *et al.*, 2006). Only 5% of the existing tsunami literature is related to palaeotsunamis (Scheffers & Kelletat, 2003). This can be due to ambiguous distinguishing features (Morton *et al.*, 2007; Dawson & Stewart, 2008; Bahlburg & Spiske, 2012), which make tsunami deposits difficult to discriminate from storm deposits (Bruzzi & Prone, 2000; Bryant & Nott, 2001; Witter *et al.*, 2001; Pratt, 2002; Tuttle *et al.*, 2004; Goff *et al.*, 2004; Nigam & Chaturvedi, 2006; Kortekaas & Dawson, 2007). Features used to distinguish the offshore products of

tsunami activity include sediment texture (Pratt, 2002), taphonomic features (Puga-Bernabéu & Aguirre, 2017), and exotic marine microfauna (Nigam & Chaturvedi, 2006; Mamo *et al.*, 2009) and macrofauna (Massari *et al.*, 2009). Additional clues identifying marine tsunami deposits encompass indications of successive sedimentation pulses: alternating coarse (high-energy) and fine (decantation) layers (Bondevik *et al.*, 1997; Fujino *et al.*, 2006; Fujiwara & Kamataki, 2007) and sedimentary structures such as pebble imbrications and cross-stratification formed by ripples and dunes indicating bipolar current directions (Massari & D'Alessandro, 2000; Lawton *et al.*, 2005; Fujino *et al.*, 2006; Fujiwara & Kamataki, 2007). In addition, tsunamigenic soft-sediment deformation of the sea floor is common (Rossetti *et al.*, 2000; Takashimizu & Masuda, 2000; Schnyder *et al.*, 2005; Puga-Bernabéu *et al.*, 2007).

Tsunamis lead to rapid coastal inundation and energetic backwash (Le Roux & Vargas, 2005; Nanayama & Shigeno, 2006; Feldens *et al.*, 2009, 2012; Paris *et al.*, 2010; Bahlburg & Spiske, 2012). Most attention has been paid to tsunami deposits in onshore siliciclastic settings (Dawson & Stewart, 2007), which generally show normal grading and landward-fining and thinning trends (Hindson & Andrade, 1999; Nanayama *et al.*, 2000; Gelfenbaum & Jaffe, 2003; Goff *et al.*, 2004; Tuttle *et al.*, 2004; Moore *et al.*, 2006; Fujino *et al.*, 2010; Bahlburg & Spiske, 2012) and often contain allochtonous foraminifers (Okahashi *et al.*, 2002; Nanayama & Shigeno, 2006; Kortekaas & Dawson, 2007; Mamo *et al.*, 2009; Uchida *et al.*, 2010). In addition, large boulders of more than 1000 tonnes can be brought hundreds of metres inland (Scheffers & Kelletat, 2003). Marine deposits formed by tractive backwash currents (Dawson & Stewart, 2008), on the other hand, have been relatively rarely studied (Shiki & Yamazaki, 1996; Massari & D'dro, 2000; Rossetti *et al.*, 2000; Fujino *et al.*, 2006; Fujiwara & Kamataki, 2007; Puga-Bernabéu *et al.*, 2007; Puga-Bernabéu & Aguirre, 2017) despite their greater preservation potential (Einsele *et al.*, 1996). Tsunami backwash is associated with strong currents capable of bringing sediment from the inundated land to (shallow) marine environments (Dawson & Stewart, 2008). Such strong return flows were previously suggested to have induced the formation of large-scale (tens of metres) undulations floored with scours (Bartsch-Winkler & Schmoll, 1984; Moore & Moore, 1988; Galli, 1990; Massari & D'Alessandro, 2000; Rossetti *et al.*, 2000; Bussert & Aberhan, 2004; Puga-Bernabéu *et al.*, 2007) and antidune deposits in offshore settings (Shiki & Yamazaki, 1996; Smit *et al.*, 1996; Massari & D'Alessandro, 2000; Fujiwara & Kamataki, 2007; Ishihara *et al.*, 2014).

Numerical simulations offer a powerful tool that complements the understanding of tsunamigenic sediment transport dynamics (Xiao *et al.*, 2010; Apotsos *et al.*, 2011a; Gusman *et al.*, 2012; Kihara *et al.*, 2012; Ranasinghe *et al.*, 2013; Sugawara *et al.*, 2014), demonstrating that the backwash current normally operates in a Froude-supercritical flow regime (Simpson & Castelltort, 2006; Weiss, 2008; Apotsos *et al.*, 2011b; Yamazaki *et al.*, 2011; Jiang *et al.*, 2015), which is consistent with observations from laboratory flume experiments (Yoshii *et al.*, 2017) and calculations of flow parameters of real-world tsunamis (Bahlburg & Spiske, 2012). Rapid deceleration of the supercritical flow, e.g. upon reaching the sea or running over a slope break (Yamazaki *et al.*, 2011), forces the transition to subcritical conditions accompanied by high rates of suspension fallout (Apotsos *et al.*, 2011b) and the formation of a hydraulic jump (Simpson & Castelltort, 2006; Weiss, 2008; Yamazaki *et al.*, 2011; Jiang *et al.*, 2015). While supercritical backwash may transport large amounts of sediment, the transition from the supercritical return flow to the sluggish, landward-migrating hydraulic jump may be the most important element of deposition of tsunami sediment transported seawards.

This study discusses marine tsunamigenic backwash and presents a process-based analysis of an inferred tsunami deposit from the Lower Pleistocene on Rhodes Island (Greece). A set of diagnostic features for recognizing high-energy, marine backwash deposits in the geological record is presented. Part of the studied outcrop is interpreted as being the result of tsunamis on the basis of their position within decimetric, bioturbated higher-frequency, storm-induced beds. The inferred tsunami beds have larger volumes (metre-scale thickness), they lack bioturbation in the basal and central part, and are associated with higher-energy conditions indicated by the presence of backset-beds (antidune cross-bedding). In particular, the supercriticality of tsunami-backwash currents and the transition to subcriticality accompanied by a hydraulic jump and large-scale deposition of sediment are considered here. This has been a largely ignored criterion of tsunamigenic depositional processes.

GENERAL TSUNAMI CHARACTERISTICS

Generation by disturbance of the water column

Tsunamis are generated in four ways (Sugawara *et al.*, 2008; Bourgeois, 2009). Earthquakes lie at the origin of most: 90% worldwide and 75% in the Mediterranean Sea (Sugawara *et al.*, 2008; Sørensen *et al.*, 2012). Volcanic eruptions (e.g. Santorini and Krakatoa, Latter, 1981; Cita & Aloisi, 2000) and (subaqueous) landslides (e.g. Storegga and Hawaii, Bondevik *et al.*, 1997; Ward, 2001; McMurtry *et al.*, 2004; Puga-Bernabéu *et al.*, 2013) are other important contributors. A minor number of tsunamis

have been caused by bolide-water impacts (Ward & Asphaug, 2000; Kharif & Pelinovsky, 2005), the most famous undoubtedly being the asteroid impact at the Cretaceous-Palaeogene boundary (Smit *et al.*, 1996), suggested to have induced a mega-tsunami, exceeding 150 m in height, which travelled as far as 300 km inland (Matsui *et al.*, 2002), leading to backwash over a period of hours or even days (Lawton *et al.*, 2005). Scheffers and Kelletat (2003) report over 50 historical occurrences worldwide of run-up heights of more than 10 m, with five exceeding 100 m, during the last 400 years. Numerical modelling on the basis of a synthetic earthquake database by Sørensen *et al.* (2012) reveals a probability of close to 100% for a tsunami wave run-up exceeding 1 m to occur somewhere along the Mediterranean coast every 30 years.

Propagation from deep into shallow water

Deep-water tsunami waves have very long wavelengths (exceeding 100 km) and propagate at hundreds of km/h (Joseph, 2011). Tsunami wave periods range from 10 min to 1 h, that is, some 100 times longer than the period of wind-induced waves (Weiss & Bahlburg, 2006; Fujiwara, 2008). Tsunami waves slow down when they reach shallower water, while wave amplitude and current velocity (uniform throughout the water column) increase (Sugawara *et al.*, 2008; Joseph, 2011), in agreement with eyewitness accounts and video footage of a landward moving 'wall of water' (Tappin *et al.*, 2012). Such bores move over a basal boundary layer where most of the shear stress is generated, capable of transporting virtually all grain sizes (Pickering *et al.*, 1991; Weiss, 2008). This produces a distinctive flow style (Dawson, 1994) characterized by (i) a widespread uprush associated with coastal impact, (ii) a quasi-stillstand when the current stagnates and (iii) a vigorous backwash during water retreat, each stage lasting many minutes or longer. This cycle can be repeated multiple times as a consequence of the tsunami wave train, with hydraulic energy generally decreasing with each new incursion (Sugawara *et al.*, 2008), although this is not always the case (Nanayama & Shigeno, 2006). Shiki and Yamazaki (1996) pointed out that tsunamis generated very close to the hypocentre of an earthquake are generally marked by only a few pulses. In certain cases, the backwash of the second wave stopped the propagation of the following waves (Lavigne *et al.*, 2009).

Inundation of onshore area

The process of tsunami wave impact at the shore is essentially similar to that of normal waves at the beach (Butt & Russell, 1999; Young *et al.*, 2010), characterized by rapid flow acceleration as the wave front passes (Apotsos *et al.*, 2011b). Associated erosion may extend up to hundreds of metres inshore, and much farther along river beds (Ontowirjo *et al.*, 2013). Tsunami run-up velocities may be as high as 10 to 18 m s^{-1} (35 to 65 km h^{-1}; Reimnitz & Marshall, 1965; Tsutsumi *et al.*, 2000; Bryant & Nott, 2001), in particular in narrow channels and near headlands (Cherniawsky *et al.*, 2007). The erosional phase is followed by a depositional phase during gradual deceleration until the point of maximum inundation is reached (Apotsos *et al.*, 2011b). Tsunamis are thus both depositional and erosional agents (Dawson, 1994). Whether erosion or deposition predominates depends largely on the erosion capacity of the backwash current (Umitsu *et al.*, 2007). As a consequence of flow deceleration, deposits formed by the onshore tsunami uprush are typically graded, and thin and fine landwards (Hindson & Andrade, 1999; Nanayama *et al.*, 2000; Gelfenbaum & Jaffe, 2003; Goff *et al.*, 2004; Tuttle *et al.*, 2004; Moore *et al.*, 2006; Fujino *et al.*, 2010; Bahlburg & Spiske, 2012) and are commonly capped by organic-rich mud layers laid down during tsunami stillstand at maximum inundation (Tuttle *et al.*, 2004; Morton *et al.*, 2007; Fujiwara, 2008). Large, occasionally imbricated boulders located hundreds of metres onshore have also been ascribed to the energetic uprush phase (Goto *et al.*, 2007; Frohlich *et al.*, 2009; Maouche *et al.*, 2009). The inland propagation after coastal impact is thus well beyond the normal position of the shoreline, up to hundreds of metres for steep coastal areas (generally coarse-grained) and up to kilometres where the coastal gradient is low (fine-grained) (see compilation by Scheffers & Kelletat, 2003). Tsunami wave energy, height and velocity are considerably reduced in the presence of coastal vegetation, e.g. by flow resistance in mangrove forests (Teh *et al.*, 2009) or as a result of energy loss due to tree breaking (Thuy *et al.*, 2012), and is therefore a focus of tsunami-impact mitigation programmes.

Backwash from inundated onshore areas into shallow-marine waters and beyond

Bottom friction, percolation of water into the ground and energy loss due to the run-up eventually cause the cessation of the landward advance of tsunamis. As a consequence of the wave retreating faster than the receding water (Yamazaki *et al.*, 2011), a subsequent reverse flow develops after a short period of stagnation (Dawson & Stewart, 2008), while tsunami water near the shoreline starts to retreat before the maximum inundation height is reached and the wave front continues to move onshore (Apotsos *et al.*, 2011b). Resulting tractive backwash currents become concentrated towards topographic lows (Einsele *et al.*, 1996; Le Roux & Vargas, 2005; Li *et al.*,

2012; Fujiwara & Tanigawa, 2014) and might locally erode bed rock platforms (Aalto *et al.*, 1999). Coastal relief can cause the backwash to flow obliquely to the shoreline. Such local factors have different effects on each of the sub-units of a tsunami deposit (Fujino *et al.*, 2006), potentially resulting in high lateral variability in the associated sediment. Similarly, rebound from coastal cliffs influences the distribution of the backwash deposit (Massari & D'Alessandro, 2000).

Numerical simulations show that the erosion capacity of the backwash depends on the amount of water onshore, which is a function of tsunami wave height (Fagherazzi & Du, 2008) and the slope of the bed (Apotsos *et al.*, 2011b). Along high-relief coastlines, tsunami backwash is accelerated due to gravity, gaining transport potential and the ability to generate net offshore transport especially in the case of well-erodible substrates (MacInnes *et al.*, 2009). As a consequence, backwash-generated erosion rates achieved seawards of the shoreline (on parts of the sea floor that are normally below sea-level) are potentially much higher than onshore (Pritchard & Dickinson, 2008; Apotsos *et al.*, 2011b; Li *et al.*, 2012). Accordingly, several field surveys show that tsunamis were net depositional on low-relief coastlines (Gelfenbaum & Jaffe, 2003; Kurian *et al.*, 2006), whereas tsunamis flowing over high-relief coastlines generated net offshore transport (MacInnes *et al.*, 2009).

Modelling and calculations demonstrate that the backwash develops into a supercritical flow, also on low-gradient coasts (Simpson & Castelltort, 2006; Weiss, 2008; Apotsos *et al.*, 2011b; Bahlburg & Spiske, 2012; Jiang *et al.*, 2015; Yoshii *et al.*, 2017). Rapid deceleration upon entering the sea invokes high settling rates of suspended sediment that may lead to the formation of hyperpycnal flows (Coleman, 1968; Le Roux & Vargas, 2005; Weiss, 2008), particularly where coastal funnelling of receding tsunami water occurs. Coleman (1968) suggested a link between coastal funnelling and the formation of submarine canyons, generating and expanding pathways for turbidity currents. Some authors have questioned whether the deposits of self-sustained tsunamigenic density flows, which have lost a direct connection with the tsunami backwash, should be considered 'tsunamiites' (Shanmugam, 2006; Weiss, 2008). Such self-sustained density flows are beyond the scope of this study.

Because backwash flows are characterized by an initial waxing and final waning stage (Apotsos *et al.*, 2011b; Yoshii *et al.*, 2017), their deposits commonly encompass graded beds overlying an erosional base (Dawson, 1994; Nanayama *et al.*, 2000; Fujino *et al.*, 2006; Nanayama & Shigeno, 2006; Fujiwara & Kamataki, 2007; Bahlburg & Spiske, 2012). Thus, sediment deposited onshore during the run-up and stagnation phases and the evidence of landward-directed currents are potentially removed or reworked during backwash. Rare descriptions of backwash-generated deposits on land document mainly structureless to graded sand and gravel, in the case of Bahlburg and Spiske (2012) forming widespread prograding fans in the lee of terrace steps. Such onshore backwash deposits locally include seaward-directed cross-bedding and current ripple lamination (Nanayama & Shigeno, 2006; Bahlburg & Spiske, 2012) and landward-imbricated gravel (Nanayama *et al.*, 2000; Bahlburg & Spiske, 2012). In the marine realm, "scour-and-graded" backwash beds (Fujino *et al.*, 2006; Fujiwara & Kamataki, 2007) reflecting the progressive decrease in hydraulic energy of the backwash. In addition to grading, marine tsunami-backwash deposits comprise a variety of sedimentary structures such as ripple and dune cross-stratification, upper plane-bedding, antidune lamination and hummocky cross-stratification (HCS) (Lawton *et al.*, 2005; Fujiwara *et al.*, 2000; Fujiwara & Kamataki, 2007), including large-scale (up to 50 m wavelength) scour-and-fill structures (Massari & D'Alessandro, 2000; Rossetti *et al.*, 2000; Fujino *et al.*, 2006; Puga-Bernabéu *et al.*, 2007). Such offshore tsunami beds are typically interbedded with the deposits of marine background sedimentation.

EXAMPLE OF MARINE BACKWASH DEPOSITS ON RHODES ISLAND

In the following section a candidate for marine tsunami-backwash deposits in coarse-grained, mixed carbonates from the Lower Pleistocene on Rhodes Island (Greece) is described (Fig. 1). The exposures enable a process-based analysis of high-energy event deposits in an otherwise low-energy shallow-marine environment. These deposits, previously studied by Hansen (1999), form part of the Cape Arkhangelos Calcarenite facies group of the Rhodes Formation. The depositional setting adhered to in this study is strongly based on the work of Hansen (1999), however, his Facies C, D and E are here combined and reinterpreted together.

Depositional setting

Rhodes Island is located in the Aegean Sea on the eastern reach of the Hellenic Arc, a chain of forearc islands north of the Hellenic subduction zone (Fig. 1). On the east coast of Rhodes, Plio-Pleistocene extensional grabens developed in Mesozoic meta-limestones (Hanken *et al.*, 1996). The Lower Pleistocene Cape Arkhangelos Calcarenite discussed here was deposited in an E-W trending basin, bounded to the N and NE by a steep, cliffed headland of the meta-limestone 'basement', and to the S and W by Pliocene siliciclastics (Hansen, 1999). In a small embayment near Kallithea Springs (Fig. 1), a temperate

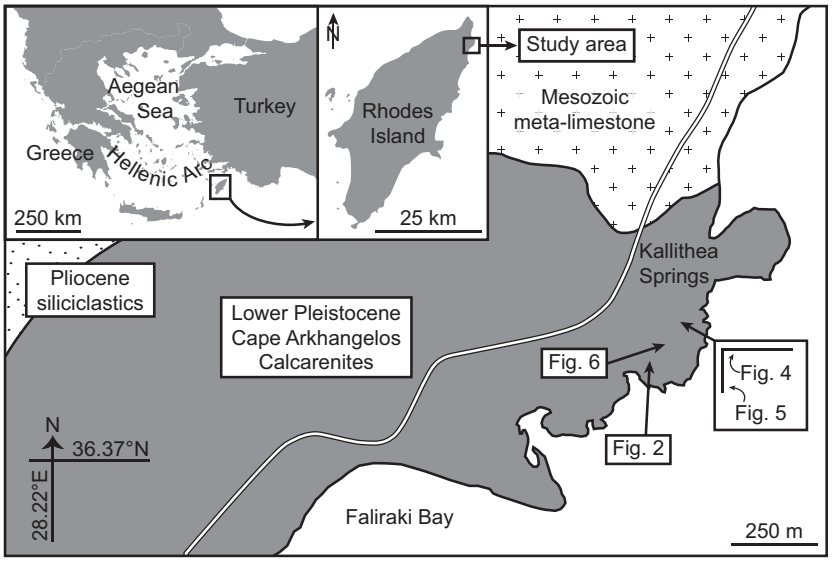

Fig. 1. Location of the study area near Kallithea Springs on the island of Rhodes in the eastern Mediterranean Sea (after Hansen, 1999). The Lower Pleistocene Cape Arkhangelos Calcarenites discussed here were deposited in a relatively small embayment.

carbonate platform developed during the Early Pleistocene. During its build-up phase, the platform was greatly influenced by the input of siliciclastic sediment, which was gradually replaced by biogenic debris as the platform matured. Skeletal production rates eventually exceeded the creation of accommodation space and excess carbonate sediment was occasionally transported seawards and deposited on the sloping front of the prograding wedge that separated the upper and lower shoreface, leading to the formation of the "giant-scale foresets" of Facies E of Hansen (1999). The generally very well-sorted clinoform foresets are 5 to 100 cm thick and up to 12 m high with a variable dip (5 to 40°) of 10 to 15° on average (Fig. 2), consisting of cross-bedded and bioturbated decimetric packstone and grainstone beds (Hansen, 1999). Sediment is composed of fine-grained to medium-grained skeletal sand of dominantly rhodalgal origin and of *ca* 10% lithic components (Fig. 3). Centimetre-scale rhodolith fragments occur sporadically.

Scour-and-fill structures

The succession of clinoform foresets contains more than 20 spoon-shaped scour-and-fill structures some 10 to 80 m wide (Hansen, 1999) with variable longitudinal dimensions, occurring at various stratigraphic positions. Outcrop conditions impede the detailed mapping of all scour-and-fill structures. The studied exposure displays two such, broadly similar structures each made up of three sub-units (Figs 3 and 4). The lower scour-and-fill structure (Unit 1) is exposed over 25 m in approximately palaeoflow-parallel direction. It is up to 5 m thick and has an erosional base with steep side walls and up to 3 m of local relief (Figs 4 and 5). Unit 1 is overall fining upwards with much coarser sediment than the clinoform foresets (Fig. 3). In contrast to the locally intensely bioturbated packstones and grainstones of the clinoform foresets, Sub-units 1 and 2 and the lower part of Sub-unit 3 are devoid of bioturbation, which only affected the upper part of Sub-unit 3. The proportion of sub-angular to rounded lithic components ranges from as much as 2/3 at the base to about 1/4 at the top of Unit 1. The skeletal composition is invariably dominated by rhodalgal fragments, making up 20 to 30% of the bioclastic grains (Fig. 3). Each sub-unit is described in more detail:

Sub-unit 1

Backset-bedded conglomerate. Backset-beds (Davis, 1890) within this sub-unit are up to 20 cm thick and dip up to 50° (exceeding the angle of repose indicating rapid covering) in a landward direction. They have sigmoidal shapes with a convex-up seaward end and a concave-up base where each backset-bed truncates the underlying one, generating the erosion surface that floors the entire scour-and-fill structure of Unit 1 (Fig. 4). Individual backset-beds are poorly sorted, while grain size decreases seawards yet remaining within the conglomerate range. As a result of the seaward-fining trend within individual backset-beds, Sub-unit 1 is fining upwards. The decrease in grain

Fig. 2. Lower Pleistocene prograding mixed carbonate wedge on Rhodes Island. Packstone and grainstone clinoform foresets are up to 12 m high. See Fig. 1 for location (N36·375067° E28·236374°). Dashed line marks the erosional contact with the unconformable overlying deposits (cf. Hansen, 1999). Person (185 cm) indicates the scale.

size is accompanied by a reduction in the proportion of lithic components, decreasing from *ca* 2/3 at the base to 1/3 at the top of the sub-unit. In exposures perpendicular to the palaeoflow, Sub-unit 1 displays lenticular geometries marked by numerous reactivation surfaces (Fig. 6).

Sub-unit 2

Wavy-bedded grainstone. This sub-unit consists of undulating, centimetric planar bedding that truncates the top of Sub-unit 1. The bedding is similar to that produced by upper plane-flow, but develops vertically into low-angle foreset cross-bedding towards the top of Sub-unit 2. The sediment is composed of well-sorted, coarse sand of which *ca* 1/5 is of lithic origin. Locally, internal truncations occur (Fig. 4).

Sub-unit 3

Cross-bedded rudstone. The low-angle foreset cross-bedding of the upper part of Sub-unit 2 passes vertically into the much steeper cross-bedding of the more voluminous Sub-unit 3. In both sub-units, cross-bedding dips uniquely in seaward direction. The moderately sorted rudstones form decimetric sets that together reach over 3 m in thickness. The granule-size sediment in Sub-unit 3 is for *ca* 1/4 composed of lithic fragments. The upper half is generally affected by vertically intensifying bioturbation.

Process interpretation

Each scour-and-fill unit was deposited from an overall waning, seaward-directed flow that went through a series of distinct hydrodynamic conditions and deposition of associated sub-units (Fig. 7): (1) hydraulic jump depositing coarse-grained backset-beds, (2) sheet-flow generating upper plane bedding and (3) highly depositional subcritical flow leading to the aggradational stacking of subaqueous dunes. The high proportion of lithic components in the scour-and-fill structures, when compared to that in the clinoform foresets, attests to a sediment source near the shoreline (or on land) mixed with shallow-marine-derived skeletal grains. This matches well with an origin from a very strong marine backwash event following coastal inundation. Backwash-generated erosion left a substantial imprint in the sedimentary record. The erosion surface at the base of Unit 1 is the result of rapid alternations of erosion and deposition: First, an individual backset-bed was 'dumped' during the depositional phase. Then, during the intermittent erosion phase, part of the clinoform foreset and part of the landward side of the backset-bed just deposited were eroded. Prolonged repetition of these two alternating phases generated the backset-beds of Sub-unit 1, which is thus floored by a composite erosion surface (Fig. 4) (cf. Dietrich *et al.*, 2016; Slootman *et al.*, 2016) that formed as a result of the intrinsic, high-frequency pulsating nature of the supercritical backwash current rather than due to the impact of the landward-migrating wave(s).

Thus, the composite erosion surface at the base of Sub-unit 1 formed as the result of high basal shear stresses in a supercritical flow that ran down the bathymetric break separating the upper and lower shoreface. Where this surface flattened and the flow decelerated and thickened, a convex-up antidune was created under stationary wave conditions (Fig. 7). The generation of such an obstacle resulted in the vertical growth of a standing wave until oversteepening and subsequent breaking occurred, resulting in the formation of a hydraulic jump (cf. Alexander *et al.*, 2001; MacDonald *et al.*, 2009; Cartigny *et al.*, 2014; Slootman, 2016). Alternatively, the initial sediment mound was deposited directly from the hydraulic jump by suspension fallout due to the rapid loss of traction (cf. MacDonald *et al.*, 2009). The hydraulic jump migrated upstream and upslope by the continued deposition of locally very steep backset-beds (Sub-unit 1) that formed by the massive settling of coarse sediment directly downstream of the jump (Fig. 7) (cf. Massari, 1996). The length and inclination of the slope over which the supercritical flow accelerated thereby progressively decreased

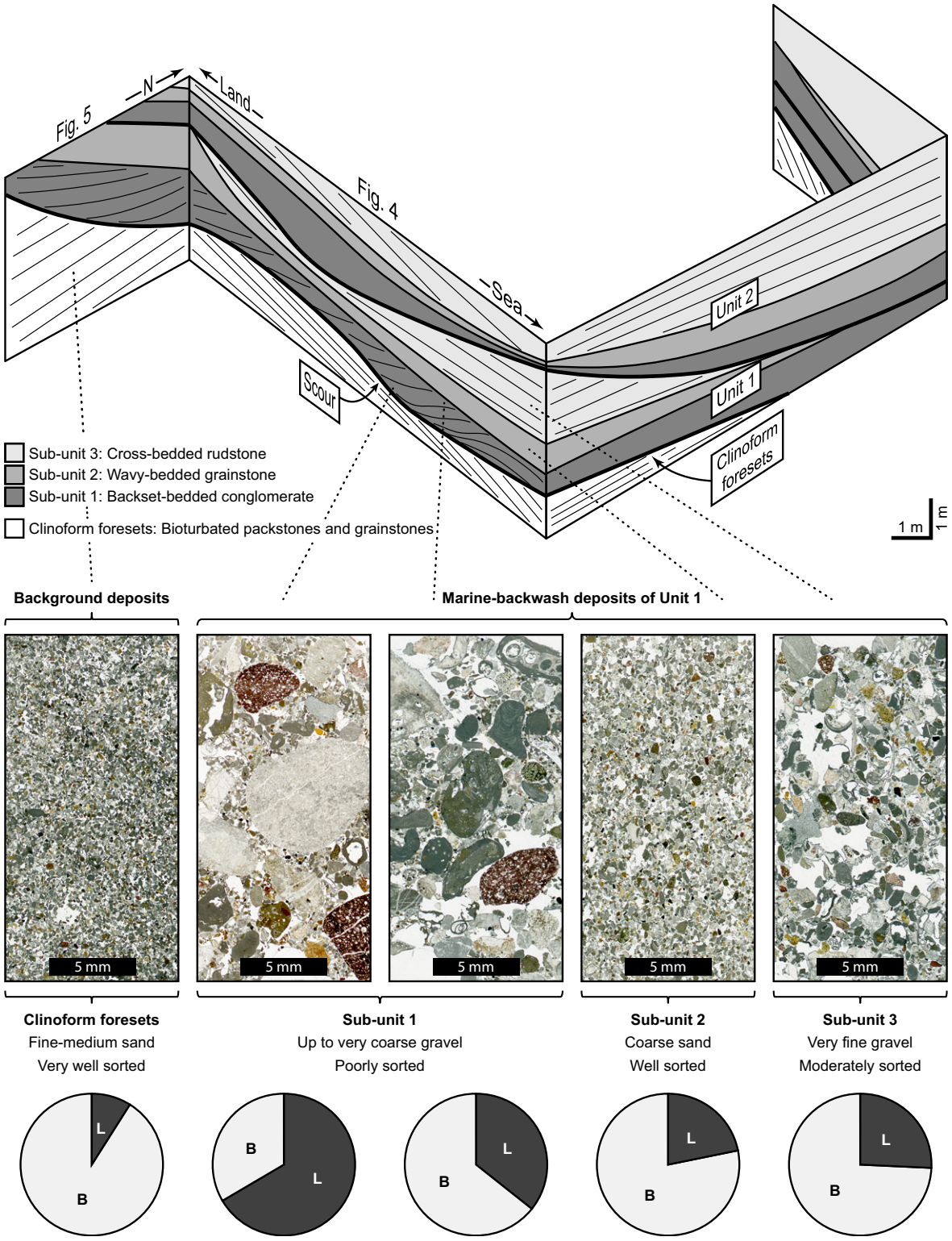

Fig. 3. Schematic overview of the studied outcrop, showing clinoform foresets incised by two scour-and-fill structures (Units 1 and 2). Each unit consists of three sub-units. A detail of representative thin sections for the clinoform foresets and each of the sub-units are displayed. Circle diagrams indicate the proportion of bioclasts (B) and lithic components (L). See Fig. 1 for location (N36·375893° E28·237357°).

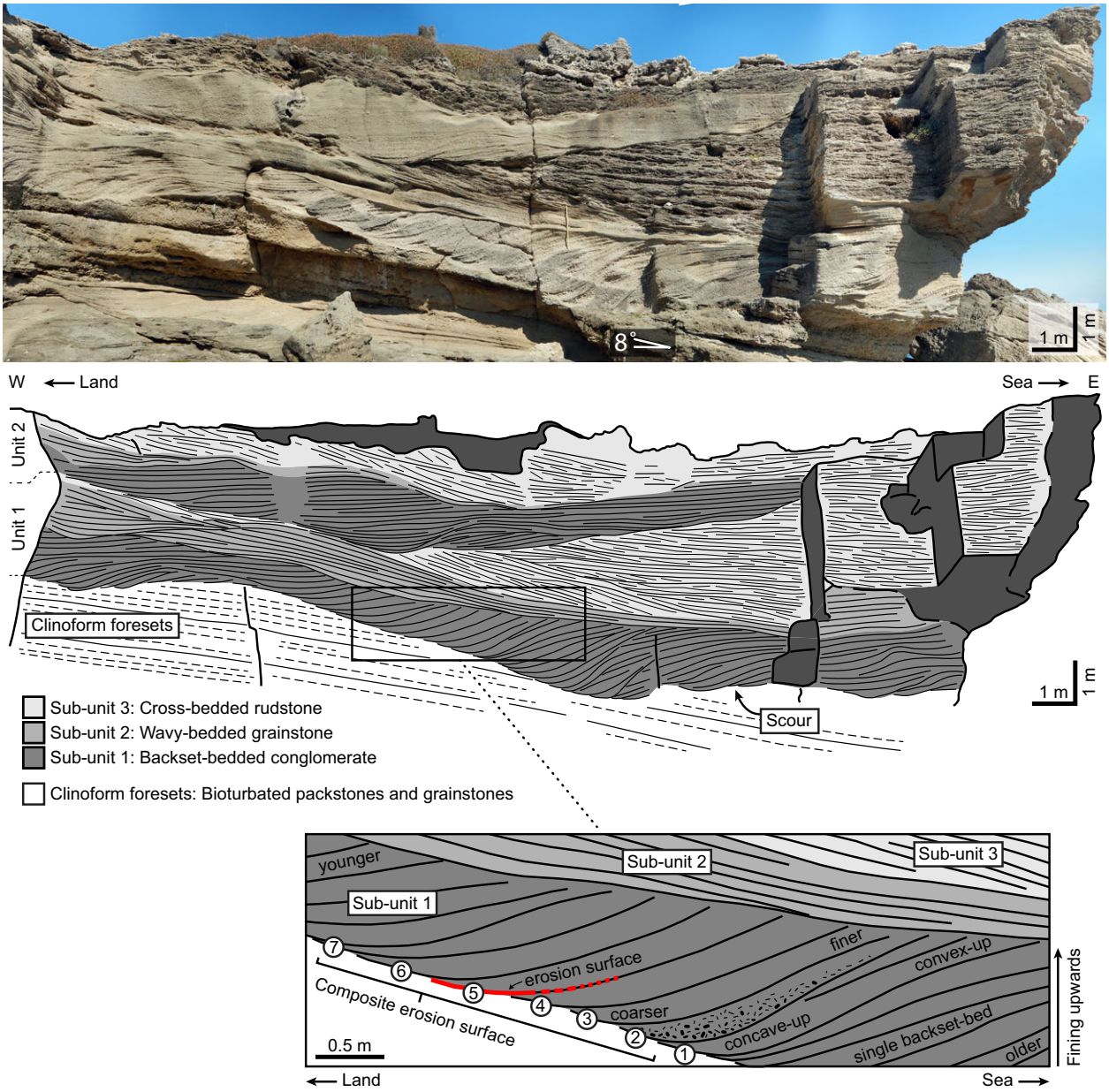

Fig. 4. Photograph and line drawing of the tri-partite scour-and-fill structures of Unit 1 and Unit 2. Internally, note that Sub-unit 1 grades vertically into Sub-units 2 and 3. The inset shows a close-up of Unit 1, demonstrating that the individual backset-beds of Sub-unit 1 are sigmoid-shaped, fine upwards and seawards, and terminate in a concave-up erosion surface at their base. These erosion surfaces together form the irregular composite erosion surface (scour) that floors Unit 1. Encircled numbers indicate the relative timing of the formation of erosion surfaces. The exposure is approximately parallel to the palaeoflow direction. See Figs 1 and 3 for location.

and, as a result, so did the intensity of the hydraulic jump (decreasing difference between Froude numbers at either side of the jump). This induced the transition to subcritical flow conditions throughout the slope and upper-stage plane-bed formation (Sub-unit 2). Further gradual decrease in hydraulic energy led to relatively sustained flow conditions with high rates of sediment fallout from the sediment-laden flow and the formation of subaqueous dunes (Sub-unit 3). Bioturbation of the upper half of Sub-unit 3 started after deposition. At this location, the event deposit consists of only one waning-flow deposit. If the event was associated with multiple waning-flow phases, these did not leave a sedimentary imprint at this particular location.

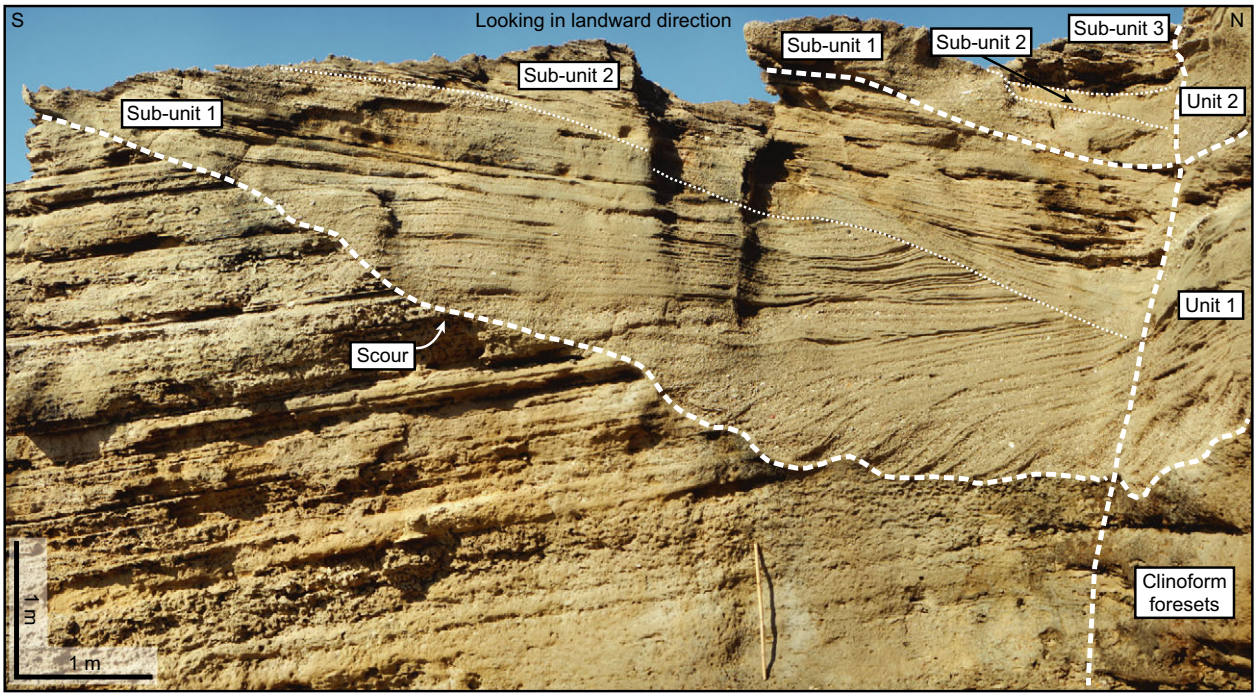

Fig. 5. Scour-and-fill structures of Units 1 and 2 from Figs 3 and 4 here cut approximately perpendicular to the palaeoflow direction. Note the irregular erosion surface (scour) at the base of Sub-unit 1, outlining the spoon-shaped geometry of Unit 1. See Figs 1 and 3 for location.

DISCUSSION

Marine tsunami-backwash deposits

Backset-stratification similar to that of Sub-unit 1 and wavy bedding such as in Sub-unit 2 have been reported from ancient sediments elsewhere and were ascribed to deposition from hydraulic jumps and antidune-like processes (Postma *et al.*, 1983; Nemec, 1990; Massari, 1996; Pomar *et al.*, 2002; Breda *et al.*, 2007; Duller *et al.*, 2008; Lang & Winsemann, 2013; Gobo *et al.*, 2014; Dietrich *et al.*, 2016; Slootman *et al.*, 2016; Massari, 2017; Ono & Plink-Björklund, 2017). The occasional oversteepening of scour-side walls and backset-beds, exceeding the angle of repose for granular material, such as also documented on fossil carbonate ramps on Sicily (Slootman, 2016), was attributed to the process of scouring and infilling being almost simultaneous (Hansen, 1999). Soft-sediment deformation structures associated with the scour-and-fill process were not observed in the studied outcrop, but it was noted that the clinoform foresets "have slumped during the scouring event" in a single example (Hansen, 1999).

Structures comparable to those of Sub-units 1 and 2 have also been produced experimentally by hydraulic jumps and antidunes in laboratory flumes (Simons *et al.*, 1965; Hand, 1974; Alexander *et al.*, 2001; MacDonald *et al.*, 2009; Cartigny *et al.*, 2014). It was recognized that antidune lamination may be misinterpreted as HCS (Rust & Gibling, 1990; Masuda *et al.*, 1993; Mulder *et al.*, 2009; Ono & Plink-Björklund, 2017) because both structures consist of a combination of convex and concave structures (Alexander *et al.*, 2001; Cartigny *et al.*, 2014). The HCS and associated SCS (swaley cross-stratification, Leckie and Walker, 1982) form from combined unidirectional and oscillatory flows (Harms *et al.*, 1975; Arnott & Southard, 1990; Dumas & Arnott, 2006) and are genetically different from antidune structures.

Earlier interpretations of the studied deposits on Rhodes by Hansen (1999) proposed sediment-laden underflows to have been generated as storm or flood-induced currents that accelerated down the clinoform foresets, creating a chute-and-pool bedform (Sub-unit 1) that evolved into plane beds (Sub-unit 2) and HCS as the current waned. This led Hansen (1999) to invoke major storms or hurricanes as the formative events of the scour-and-fill structures. An argument opposing such interpretation is the gradual transition between Sub-units 2 and 3, which shows that the aggradational dunes (Sub-unit 3) are part of the event deposits. In other sections, Hansen (1999) interpreted channel fills and conglomeratic cross-bedding as two additional facies, which are here for a large part included in Sub-unit 1 and to a lesser extent in

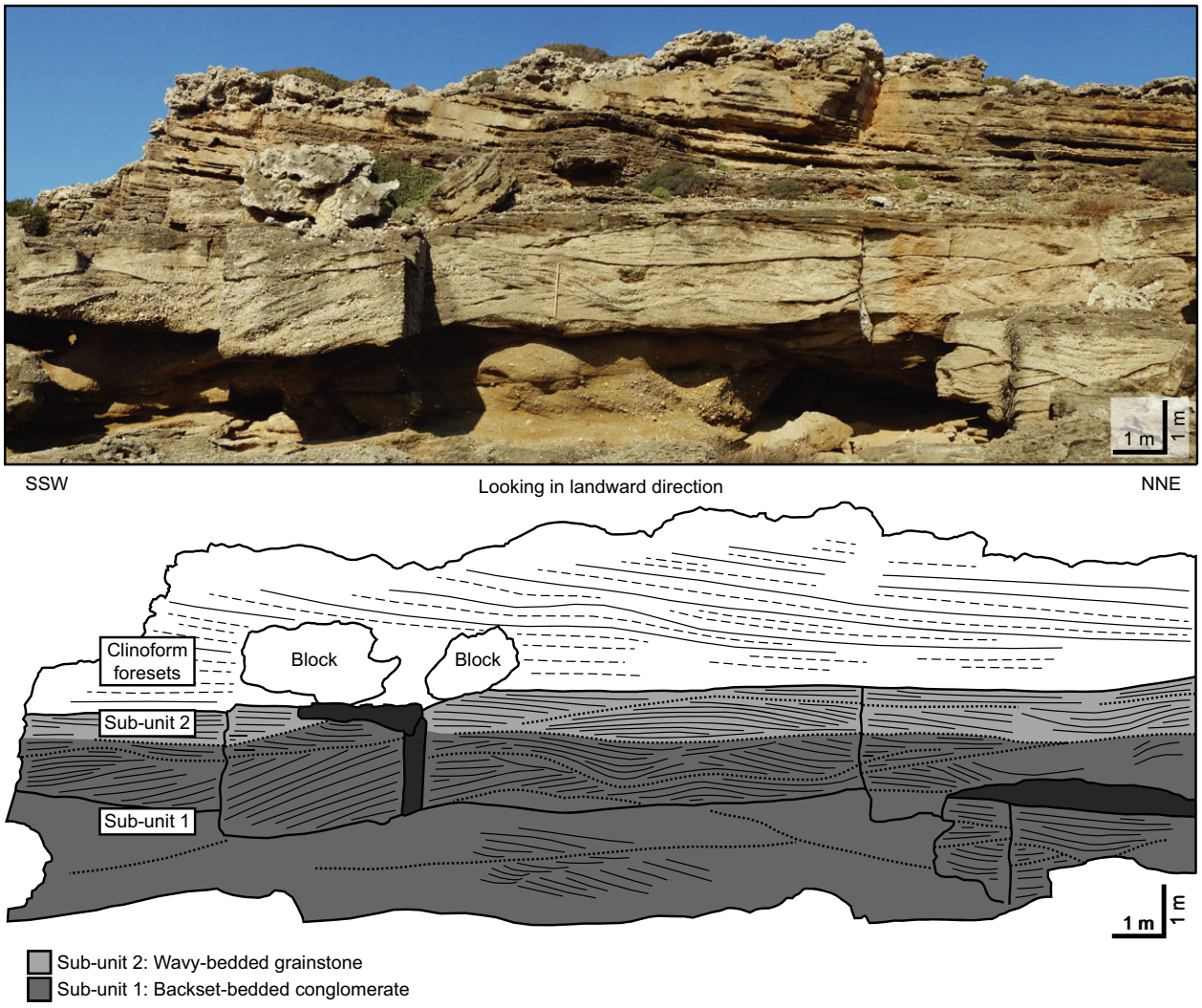

Fig. 6. Scour-and-fill structure in an approximately flow-perpendicular section (not the same unit as in Figs 4 and 5). Stippled lines indicate (erosional) subordinate set boundaries within sub-units (reactivation surfaces). Sub-unit 2 overlies Sub-unit 1. Sub-unit 3 is not exposed here. Note that the backset-bedding of Sub-unit 1 and the wavy bedding of Sub-unit 2 look like hummocky cross-stratification (HCS), but are here confidently interpreted as hydraulic jump-related and antidune-related deposits, respectively, on the basis of flow-parallel exposures. See Fig. 1 for location (N36·375734° E28·237209°).

Sub-unit 2. This illustrates the apparent ambiguity of marine backwash deposits. Likewise, cross-bedding suggested to originate from subaqueous dunes during tsunami uprush elsewhere (Nanayama & Shigeno, 2006) may indeed consist of steep backset-bedding deposited from a landward-migrating hydraulic jump during tsunami backwash such as proposed for the studied outcrops on Rhodes.

Antidune structures have been described from deep-water tsunami-induced deposits (Shiki & Yamazaki, 1996; Smit *et al.*, 1996; Ishihara *et al.*, 2014; Slootman *et al.*, 2016). In such deep-water environments, however, the generation of antidunes is no longer a direct result of tsunami backwash but is controlled by the morphodynamics of self-sustained supercritical density flows. Shallow-marine backwash deposits, on the other hand, have been reported to include HCS (Fujiwara *et al.*, 2000; Fujino *et al.*, 2006), antidune stratification (Massari & D'-dro, 2000; Lawton *et al.*, 2005) or both (Fujiwara & Kamataki, 2007). In addition, large-scale (up to 50 m wavelength) scour-and-fill structures were reported from some tsunamiites, which were in most cases characterized by smaller, superimposed scours at their base and underlain by soft-sediment deformation structures interpreted as the result of mega-hummocks formed by the combined effects of wave motion and backwash flow (Rossetti *et al.*,

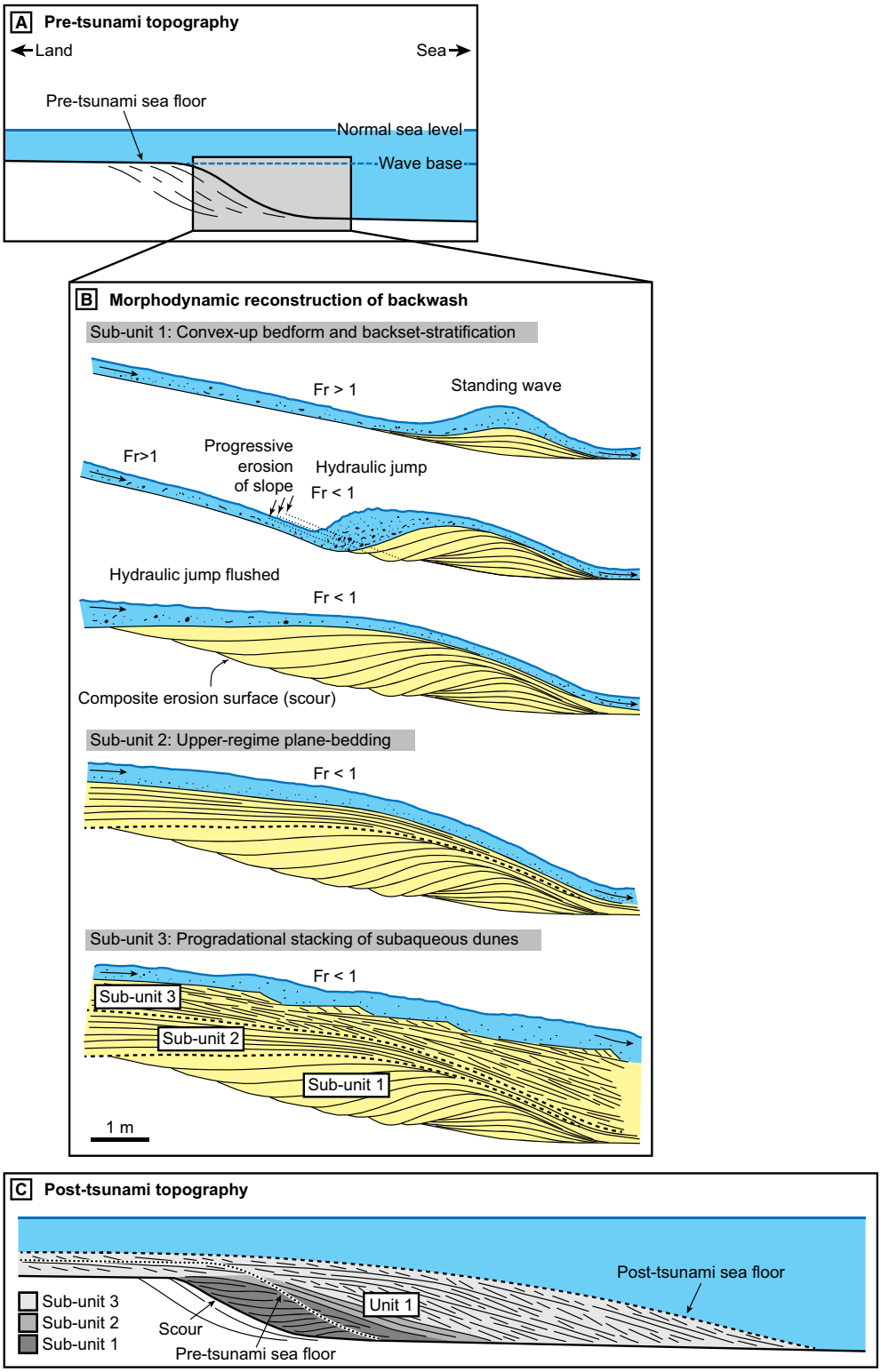

Fig. 7. Interpretive morphodynamic reconstruction of the Rhodes Island deposits. (A) Pre-tsunami sea floor. (B) Morphodynamic reconstruction of the sea floor during backwash, corresponding to the deposition of Sub-units 1 to 3 of Unit 1. (C) Post-tsunami sea floor morphology displaying Unit 1. The backwash of tsunami waves that may have occurred subsequent to the first wave left no depositional record.

2000; Fujino *et al*., 2006; Puga-Bernabéu *et al*., 2007) or, alternatively, as large-scale antidunes generated by supercritical backwash currents (Massari & D'Alessandro, 2000). The structures discussed in this study reveal the potential of the marine backwash-generated hydraulic jump in producing scour-and-fill and/or antidune structures. A more general applicability of the proposed model is investigated through a comparison with numerical simulations.

Comparison with numerical simulations of tsunami backwash

Numerical simulations can provide insight into flow processes associated with tsunami impact, uprush and backwash (Weiss, 2008; Xiao *et al*., 2010; Apotsos *et al*., 2011a,b; Gusman *et al*., 2012; Kihara *et al*., 2012; Ranasinghe *et al*., 2013; Sugawara *et al*., 2014; Jiang *et al*., 2015). Yamazaki *et al*. (2011) modelled the 2009 Samoa Tsunami in the South Central Pacific, focusing on the effect in Pago Pago Harbour located in an L-shape embayment fringed with reefs along its shores. Water depth over the *ca* 1 km long reef flat is about 10 m, increasing to 30 m over a distance of 500 m from the reef edge. The tsunami first exposed the shallow reef flats and then flooded the low-lying coastal areas in the vicinity of the harbour. Some 10 min later, the water retreated seawards and flowed supercritically over the reef edge generating a waterfall that plunged into a hydraulic jump until the next wave arrived.

Simpson and Castelltort (2006) and Jiang *et al*. (2015) incorporated sediment transport dynamics into their numerical studies to investigate the morphological evolution of the substrate during tsunamis. Both studies document supercritical backwash and the deposition of an offshore bar associated with a hydraulic jump, although neither provided details on the internal structure of the bedform. Whereas Jiang *et al*. (2015) simulated their scaled laboratory experiments, Simpson and Castelltort (2006) presented a tsunami of real-world dimensions using the one-dimensional form of the shallow-water equations (see Data S1) to compute the depth-averaged flow velocity and water depth while tracking the evolution of the substrate that evolved in response to erosion and deposition. The authors considered a typical coastal profile consisting of an initially planar, low-angle (0·2°) ramp of erodible material with a constant grain size of 4 mm that is partially emerged (Fig. 8A), which was then forced with a series of successively weaker tsunami waves (period of 15 min) arriving from the seaward end of the model (Fig. 8B through K).

To clarify the internal architecture of the backwash-generated offshore bar, the simulations of Simpson and Castelltort (2006) were repeated without changing their parameters. Tracking the topography at regular time intervals of 30 sec produced the stratification in the model (close-up in Fig. 8L). The results serve to illustrate the conceptual formative process rather than to reconstruct marine backwash in the Rhodes setting. Results show that after inundation (Fig. 8C and D), the backwash of the model tsunami is capable of transporting large quantities of sediment from the near-shore into the offshore zone as the water from each surge retreats. The sediment is initially deposited in a convex-up structure (Fig. 8E) onto which sigmoidal backset-beds accrete under a hydraulic jump at the transition between the supercritical part (at the landward side) and the subcritical part (at the seaward side) of the backwash current (Fig. 8F). The erosional concave-up bases of backset-beds deposited during the first backwash phase together form the large-scale, concave-up composite erosion surface that floors the offshore bar. Successive impact, uprush and backwash (Fig. 8G through K) did (in this case) not significantly affect the structures formed by the first tsunami cycle.

The numerically produced sedimentary structures display similarities to Sub-unit 1 in the investigated deposits, but failed to generate the wavy bedding and/or cross-bedding of Sub-units 2 and 3. In addition, the dimensions in the simulations greatly differ from those observed in outcrop. On Rhodes, the steepest backset-bed dips about 50°. In the simulations, the steepest backset-beds do not exceed a dip of 0·3°. Related to this is the difference in length between the Rhodes and model backset-beds: a few metres versus a few hundreds of metres, respectively. Such discrepancies derive indirectly from a difference in the steepness of the sea floor (*ca* 10 to 15° on Rhodes and only 0·2° in the model). A steeper sea floor leads to an increased velocity and a reduced thickness of the supercritical flow, augmenting the Froude number. The intensity of the hydraulic jump is a function of the difference in Froude number at either side of the transition. Strong jumps on steep sea floors occur over a shorter distance and are accompanied by a greater difference in flow depth between the incoming and outgoing flow. This enables the rapidly deposited fallout sediment on the steep slope to build a topographically higher bedform with backset-beds that are steeper than those associated with weaker hydraulic jumps on low-inclination sea floors. An additional effect is caused by grain-size variations. Settling velocity during tractionless suspension fallout directly downstream of the hydraulic jump increases with increasing particle diameter. This results in an enhanced sedimentation rate over a shorter distance, which thus contributes to deposition of steeper backset-beds and the formation of a bedform with shorter length and greater amplitude on steep sea floors.

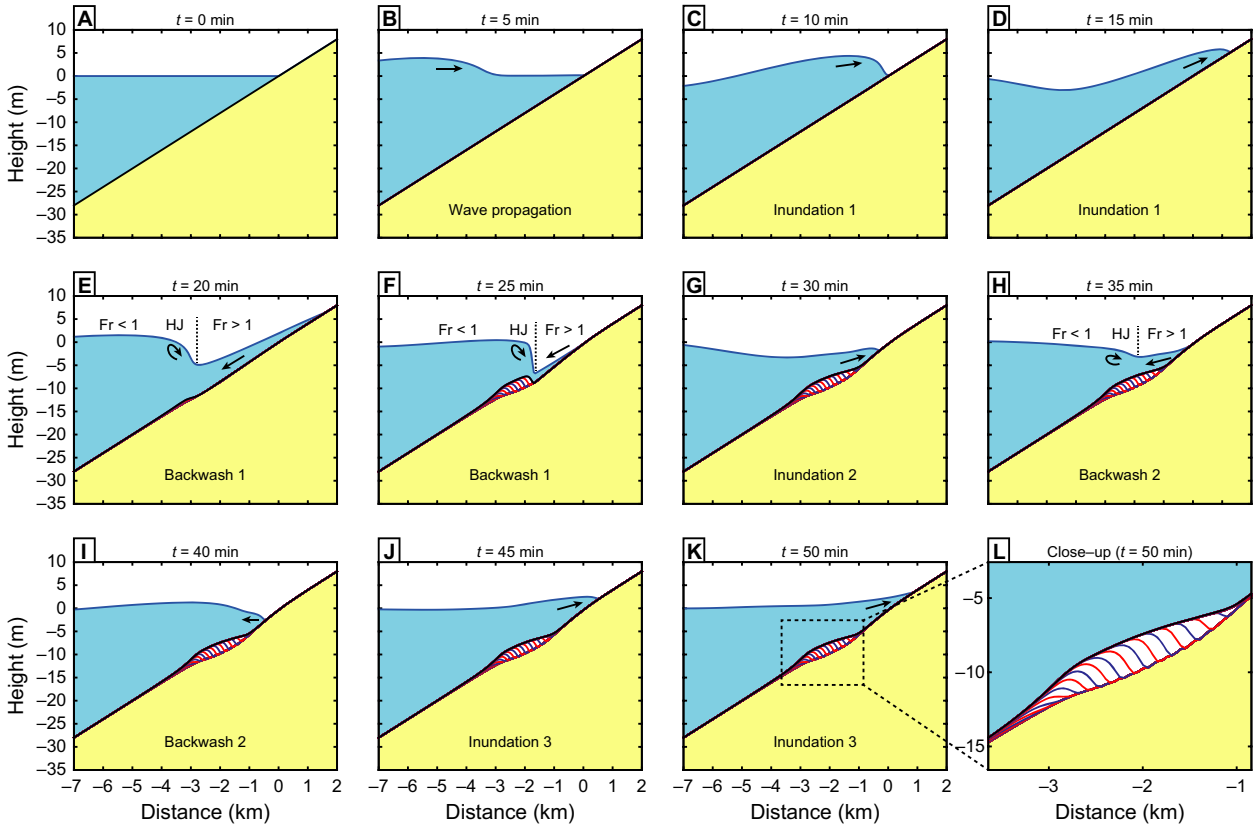

Fig. 8. Numerical simulation of Simpson & Castelltort (2006) of tsunami wave impact on a low-angle (0·2°) planar coastal profile. (A) Pre-tsunami condition. (B)-(K) Evolution of a train of tsunami waves with a wave period of 15 min, shown with 5-min time steps. Note the development of an offshore bar during the first backwash from 20 min onwards, formed under a hydraulic jump (HJ) at the transition from supercritical (Fr>1) to subcritical (Fr<1) flow. Internal stratification within this bedform was depicted by plotting the sediment–water interface with 30-sec intervals. (L) Close-up of the offshore bar, displaying internal geometries that are similar to Sub-unit 1 of the Rhodes Island marine backwash deposits, consisting of an initial convex-up bedform marked by the progressive upstream and upslope accretion of backset-strata.

Therefore, backset-stratification might only be clearly apparent in coarse-grained sediment deposited under high sedimentation rates. In finer-grained systems, and in particular in exposures with limited spatial extent, such structures may remain largely unnoticed. Field investigations by Postma *et al.* (2014) revealed low-angle backset-stratification in apparently structureless and faintly stratified Bouma Ta and Tb intervals in turbidites, deposited over large-scale bedforms (10s to 100s m wavelength) that formed in association with hydraulic jumps in turbidity currents (Postma & Cartigny, 2014). Laboratory and field observations (Postma *et al.*, 2009) demonstrated that local soft-sediment deformation within such deposits forms due to an upward-oriented pressure gradient under the hydraulic jump (see also Slootman, 2016). Therefore, while interpreting apparently structureless or faintly stratified tsunami deposits that unveil only a fining-upward signature (Takashimizu & Masuda, 2000; Fujiwara *et al.* 2000; Fujino *et al.*, 2006; Fujiwara & Kamataki, 2007), it should be considered that such deposits may have originated from a hydraulic jump during tsunami backwash, producing seemingly horizontal stratification due to the extremely low angle of the backset-beds.

Storms or tsunamis?

How can tsunami backwash deposits be discriminated from rip-current deposits generated by major storms? Tsunami features are not exclusive and a significant overlap exists between sedimentary signatures produced by cyclones and storms, including erosion surfaces, anomalously coarse sand layers, imbricated and exotic boulders, chaotic bedding, normal and inverse grading, and multiple fining-upward units (see review by Shanmugam, 2012). The repeated alternation of landward and seaward-directed currents is stressed by several authors as a main

characteristic of tsunami-induced flows (Takashimizu & Masuda, 2000; Fujiwara, 2007; Massari *et al*., 2009), however, *in situ* surveys of multiple gravity flow events demonstrate that these can also be generated during a single storm event (Puig *et al*., 2004). According to Morton *et al*. (2007), storm inundation is gradual and prolonged, marked by the impact of numerous waves onto the shore and no significant return flow until after the main flooding. In contrast, the Early Pleistocene carbonate ramp of Rhodes was affected by sudden seaward flows carrying near-shore-derived sediment (with dominantly lithic composition) mixed with shallow-marine skeletal debris. In addition, the geographical position of the island was and is within a major tsunamigenic zone, which has the greatest tsunami hazard record of the Mediterranean region, owing to the presence of nearby seismogenic faults in the Hellenic subduction zone (Lorito *et al*., 2008). Considering well-documented historical events (Papadopoulos & Fokaefs, 2005), the statistical probability of Rhodes being struck by tsunamis exceeding several metres in height is once every few centuries (Sørensen *et al*., 2012). The recurrence period of tsunamis on Rhodes is about 500 yr for tsunamis with a run-up height of 3 m and 5000 yr for run-ups 10 m high (Sørensen *et al*., 2012). The frequency of severe storm events, on the other hand, is much higher than this (Trigo *et al*., 1999; Camuffo *et al*., 2000; Leckebusch *et al*., 2006; Nissen *et al*., 2010). Hence, it is tempting to explain the clinoform foresets as the consequence of storm-induced offshore transport, and to assign tsunamis as the cause of marine backwash events that led to the generation of large-scale scour-and-fill structures.

CONCLUSION

This study stresses the potential of supercritical marine tsunami-backwash to imprint the depositional record, in particular with respect to the deposition of sediment from a hydraulic jump at the transition from supercritical to subcritical flow. Such deposits contain backset-bedding in concave-up depressions floored by composite erosion surfaces. On steep sea floors and with coarse sediment, such backset-beds build a bedform up to several metres high and of the order of 10 m long. In environments in which the coarsest grain size is sand, bedforms may be much longer and less high. As a result, the internal architecture may appear structureless or horizontally laminated due to the extreme length and very low angle of backset-beds, leaving the fining-upward signature as the only recognizable feature in typical exposure dimensions. In the view of supercritical backwash, wavy stratification is best explained as antidune stratification and not as HCS. Tsunami hazard assessment benefits from the enhanced understanding of all aspects of tsunamis. Improving the ability to recognize tsunami deposits and associated processes enables a potentially vast archive of ancient tsunamiites in the geological record to be consulted.

ACKNOWLEDGEMENTS

Paul Myrow is thanked for his review of a previous version of the manuscript. Comments by Ángel Puga-Bernabéu, an anonymous reviewer and associate editor Paul Carling are greatly appreciated and helped to improve the manuscript.

References

Aalto, K.R., Aatlo, R., Garrison-Laney, C.E. and **Ambramson, H.F.** (1999) Tsunami(?) sculpturing of the pebblebeach wave-cut platform, Crescent City area, California. *J. Geol.*, **107**, 607–622.

Alexander, J., Bridge, J.S., Cheel, R.J. and **Leclair, S.F.** (2001) Bedforms and associated sedimentary structures formed under supercritical water flows over aggrading sand beds. *Sedimentology*, **48**, 133–152.

Apotsos, A., Gelfenbaum, G., Jaffe, B., Watt, S., Peck, B., Buckley, M. and **Stevens, A.** (2011a) Tsunami inundation and sediment transport in a sediment-limited embayment on American Samoa. *Earth-Sci. Rev.*, **107**, 1–11.

Apotsos, A., Gelfenbaum, G. and **Jaffe, B.** (2011b) Process-based modeling of tsunami inundation and sediment transport. *J. Geophys. Res.-Earth*, **116**, F01006.

Arnott, R.W. and **Southard, J.B.** (1990) Exploratory flow-duct experiments on combined-flow bed configurations, and some implications for interpreting storm-event stratification. *J. Sed. Petrol.*, **60**, 211–219.

Bahlburg, H. and **Spiske, M.** (2012) Sedimentology of tsunami inflow and backflow deposits: key differences revealed in a modern example. *Sedimentology*, **59**, 1063–1086.

Bartsch-Winkler, S. and **Schmoll, H.R.** (1984) Bedding types in Holocene tidal channel sequences, Knik Arm, Upper Cook Inlet, Alaska. *J. Sed. Petrol.*, **54**, 1239–1250.

Bondevik, S., Svendsen, J.I. and **Mangerud, J.A.N.** (1997) Tsunami sedimentary facies deposited by the Storegga tsunami in shallow marine basins and coastal lakes, western Norway. *Sedimentology*, **44**, 1115–1131.

Bourgeois, J. (2009) Geological effects and records of tsunamis. In: *The Sea: Tsunamis* (Eds A.R. Robinson and E.N. Bernard), Harvard University Press, **15**, 53–91.

Breda, A., Mellere, D. and **Massari, F.** (2007) Facies and processes in a Gilbert-delta-filled incised valley (Pliocene of Ventimiglia, NW Italy). *Sed. Geol.*, **200**, 31–55.

Bruzzi, C. and **Prone, A.** (2000) Une méthode d'identification sédimentologique des dépôts de tempête et de tsunami: l'exoscopie des quartz, résultats préliminaires [A method of

sedimentological identification of storm and tsunami deposits: exoscopic analysis, preliminary results]. *Quaternaire*, **11**, 167–177.

Bryant, E.A. and **Nott, J.** (2001) Geological indicators of large tsunami in Australia. *Nat. Hazards*, **24**, 231–249.

Bussert, R. and **Aberhan, M.** (2004) Storms and tsunamis: evidence of event sedimentation in the Late Jurassic Tendaguru Beds of southeastern Tanzania. *J. Afr. Earth Sci.*, **39**, 549–555.

Butt, T. and **Russell, P.** (1999) Suspended sediment transport mechanisms in high-energy swash. *Mar. Geol.*, **161**, 361–375.

Camuffo, D., Secco, C., Brimblecombe, P. and **Martin-Vide, J.** (2000) Sea storms in the Adriatic Sea and the Western Mediterranean during the last millennium. *Clim. Change*, **46**, 209–223.

Cartigny, M.J., Ventra, D., Postma, G. and **Den Berg, J.H.** (2014) Morphodynamics and sedimentary structures of bedforms under supercritical-flow conditions: new insights from flume experiments. *Sedimentology*, **61**, 712–748.

Cherniawsky, J.Y., Titov, V.V., Wang, K. and **Li, J.Y.** (2007) Numerical simulations of tsunami waves and currents for southern Vancouver Island from a Cascadia megathrust earthquake. *Pure Appl. Geophys.*, **164**, 465–492.

Cita, M.B. and **Aloisi, G.** (2000) Deep-sea tsunami deposits triggered by the explosion of Santorini (3500y BP), eastern Mediterranean. *Sed. Geol.*, **135**, 181–203.

Clague, J.J., Bobrowsky, P.T. and **Hutchinson, I.** (2000) A review of geological records of large tsunamis at Vancouver Island, British Columbia, and implications for hazard. *Quaternary Sci. Rev.*, **19**, 849–863.

Coleman, P.J. (1968) Tsunamis as geological agents. *J. Geol. Soc. Aust.*, **15**, 267–273.

Davis, W.M. (1890) Structure and origin of glacial sand plains. *Geol. Soc. Am. Bull.*, **1**, 195–202.

Dawson, A.G. (1994) Geomorphological effects of tsunami run-up and backwash. *Geomorphology*, **10**, 83–94.

Dawson, A.G. and **Stewart, I.** (2007) Tsunami deposits in the geological record. *Sed. Geol.*, **200**, 166–183.

Dawson, A.G. and **Stewart, I.** (2008) Offshore tractive current deposition: the forgotten tsunami sedimentation process. In: *Tsunamiite* (Eds T. Shiki, Y. Tsuji, T. Yamazaki and K. Minoura), pp. 153–161. Elsevier B.V., Amsterdam, the Netherlands.

Dietrich, P., Ghienne, J.F., Normandeau, A. and **Lajeunesse, P.** (2016) Upslope-migrating bedforms in a proglacial sandur delta: cyclic steps from river-derived underflows? *J. Sed. Res.*, **86**, 113–123.

Dominey-Howes, D. (2002) Documentary and geological records of tsunamis in the Aegean Sea region of Greece and their potential value to risk assessment and disaster management. *Nat. Hazards*, **25**, 195–224.

Dominey-Howes, D. (2007) Geological and historical records of tsunami in Australia. *Mar. Geol.*, **239**, 99–123.

Dominey-Howes, D.T., Humphreys, G.S. and **Hesse, P.P.** (2006) Tsunami and palaeotsunami depositional signatures and their potential value in understanding the late-Holocene tsunami record. *Holocene*, **16**, 1095–1107.

Duller, R.A., Mountney, N.P., Russell, A.J. and **Cassidy, N.C.** (2008) Architectural analysis of a volcaniclastic jökulhlaup deposit, southern Iceland: sedimentary evidence for supercritical flow. *Sedimentology*, **55**, 939–964.

Dumas, S. and **Arnott, R.W.C.** (2006) Origin of hummocky and swaley cross-stratification – the controlling influence of unidirectional current strength and aggradation rate. *Geology*, **34**, 1073–1076.

Einsele, G., Chough, S.K. and **Shiki, T.** (1996) Depositional events and their records—an introduction. *Sed. Geol.*, **104**, 1–9.

Eisner, R.K. (2005) Planning for tsunami: reducing future losses through mitigation. *Nat. Hazards*, **35**, 155–162.

Fagherazzi, S. and **Du, X.** (2008) Tsunamigenic incisions produced by the December 2004 earthquake along the coasts of Thailand, Indonesia and Sri Lanka. *Geomorphology*, **99**, 120–129.

Feldens, P., Schwarzer, K., Szczucinski, W., Stattegger, K., Sakuna, D. and **Somgpongchaiykul, P.** (2009) Impact of 2004 tsunami on seafloor morphology and offshore sediments, Pakarang Cape, Thailand. *Pol. J. Environ. Stud.*, **18**, 63–68.

Feldens, P., Schwarzer, K., Sakuna, D., Szczuciński, W. and **Sompongchaiyakul, P.** (2012) Sediment distribution on the inner continental shelf off Khao Lak (Thailand) after the 2004 Indian Ocean tsunami. *Earth Planet Space*, **64**, 875–887.

Fraser, S., Raby, A., Pomonis, A., Goda, K., Chian, S.C., Macabuag, J., Offord, M., Salto, K. and **Sammonds, P.** (2013) Tsunami damage to coastal defences and buildings in the March 11th 2011 Mw9.0 Great East Japan earthquake and tsunami. *B. Earthq. Eng.*, **11**, 205–239.

Frohlich, C., Hornbach, M.J., Taylor, F.W., Shen, C.C., Moala, A., Morton, A.E. and **Kruger, J.** (2009) Huge erratic boulders in Tonga deposited by a prehistoric tsunami. *Geology*, **37**, 131–134.

Fujino, S., Masuda, F., Tagomori, S. and **Matsumoto, D.** (2006) Structure and depositional processes of a gravelly tsunami deposit in a shallow marine setting: Lower Cretaceous Miyako Group, Japan. *Sed. Geol.*, **187**, 127–138.

Fujino, S., Naruse, H., Matsumoto, D., Sakakura, N., Suphawajruksakul, A. and **Jarupongsakul, T.** (2010) Detailed measurements of thickness and grain size of a widespread onshore tsunami deposit in Phang-nga Province, southwestern Thailand. *Isl. Arc.*, **19**, 389–398.

Fujiwara, O. (2007) Major contributions of tsunami deposit studies to Quaternary research. *Quaternary Res.*, **46**, 293–302.

Fujiwara, O. (2008) Bedforms and sedimentary structures characterizing tsunami deposits. In: *Tsunamiite* (Eds T.

Shiki, Y. Tsuji, T. Yamazaki and K. Minoura), pp. 51–62. Elsevier B.V., Amsterdam, the Netherlands.

Fujiwara, O. and **Kamataki, T.** (2007) Identification of tsunami deposits considering the tsunami waveform: an example of subaqueous tsunami deposits in Holocene shallow bay on southern Boso Peninsula, Central Japan. *Sed. Geol.*, **200**, 295–313.

Fujiwara, O. and **Tanigawa, K.** (2014) Bedforms record the flow conditions of the 2011 Tohoku-Oki tsunami on the Sendai Plain, northeast Japan. *Mar. Geol.*, **358**, 79–88.

Fujiwara, O., Masuda, F., Sakai, T., Irizuki, T. and **Fuse, K.** (2000) Tsunami deposits in Holocene bay mud in southern Kanto region, Pacific coast of central Japan. *Sed. Geol.*, **135**, 219–230.

Galli, G. (1990) Origins of event beds in the Jurassic Calcari Grigi formation, Venetian Alps, Italy. *Geol. Mijnbouw*, **69**, 375–390.

Gelfenbaum, G. and **Jaffe, B.** (2003) Erosion and sedimentation from the 17 July, 1998 Papua New Guinea tsunami. *Pure Appl. Geophys.*, **160**, 1969–1999.

Gobo, K., Ghinassi, M. and **Nemec, W.** (2014) Reciprocal changes in foreset to bottomset facies in a Gilbert-type delta: response to short-term changes in base level. *J. Sed. Res.*, **84**, 1079–1095.

Goff, J., McFadgen, B.G. and **Chagué-Goff, C.** (2004) Sedimentary differences between the 2002 Easter storm and the 15th-century Okoropunga tsunami, southeastern North Island, New Zealand. *Mar. Geol.*, **204**, 235–250.

Goto, K., Chavanich, S.A., Imamura, F., Kunthasap, P., Matsui, T., Minoura, K., Sugawara, D. and **Yanagisawa, H.** (2007) Distribution, origin and transport process of boulders deposited by the 2004 Indian Ocean tsunami at Pakarang Cape, Thailand. *Sed. Geol.*, **202**, 821–837.

Gusman, A.R., Tanioka, Y. and **Takahashi, T.** (2012) Numerical experiment and a case study of sediment transport simulation of the 2004 Indian Ocean tsunami in Lhok Nga, Banda Aceh, Indonesia. *Earth Planet Space*, **64**, 817–827.

Hand, B.M. (1974) Supercritical flow in density currents. *J. Sed. Petrol.*, **44**, 637–648.

Hanken, N.M., Bromley, R.G. and **Miller, J.** (1996) Plio-Pleistocene sedimentation in oscillating grabens, north-east Rhodes, Greece. *Geol. J.*, **31**, 271–296.

Hansen, K.S. (1999) Development of a prograding carbonate wedge during sea level fall: Lower Pleistocene of Rhodes, Greece. *Sedimentology*, **46**, 559–576.

Harms, J.C., Southard, J.B. and **Walker, R.G.** (1975) Depositional environments as interpreted from primary sedimentary structures and stratification sequences. *SEPM Short Course*, **2**, 161.

Hindson, R.A. and **Andrade, C.** (1999) Sedimentation and hydrodynamic processes associated with the tsunami generated by the 1755 Lisbon earthquake. *Quatern. Int.*, **56**, 27–38.

Ishihara, Y., Takashimitzu, Y., Matsumoto, D. and **Mtyata, Y.** (2014) Sediment-gravity flow deposits and related deep-sea sedimentary facies along the Nichinan Coast, SE Kyrushu. *J. Geol. Soc. Jpn.*, **120**, 41–62.

Jaffe, B.E. and **Gelfenbaum, G.** (2002) Using tsunami deposits to improve assessment of tsunami risk. In: *Solutions to Coastal Disasters '02*. Conference Proceedings, ASCE, pp. 836–847.

Jiang, C., Chen, J., Yao, Y., Liu, J. and **Deng, Y.** (2015) Study on threshold motion of sediment and bedload transport by tsunami waves. *Ocean Eng.*, **100**, 97–106.

Joseph, A. (2011) *Tsunamis: Detection, Monitoring, and Early-Warning Technologies*. Academic Press, Cambridge, MA.

Kharif, C. and **Pelinovsky, E.** (2005) Asteroid impact tsunamis. *C R Phys.*, **6**, 361–366.

Kihara, N., Fujii, N. and **Matsuyama, M.** (2012) Three-dimensional sediment transport process on tsunami-induced topography changes in a harbor. *Earth Planet Space*, **64**, 787–797.

Kortekaas, S. and **Dawson, A.G.** (2007) Distinguishing tsunami and storm deposits: an example from Martinhal, SW Portugal. *Sed. Geol.*, **200**, 208–221.

Kurian, N.P., Pillai, A.P., Rajith, K., Murali Krishnan, B.T. and **Kalaiarasan, P.** (2006) Inundation characteristics and geomorphological impacts of December 2004 tsunami on Kerala coast. *Curr. Sci. India*, **90**, 240–249.

Lang, J. and **Winsemann, J.** (2013) Lateral and vertical facies relationships of bedforms deposited by aggrading supercritical flows: from cyclic steps to humpback dunes. *Sed. Geol.*, **296**, 36–54.

Latter, J.H. (1981) Tsunamis of volcanic origin: summary of causes, with particular reference to Krakatoa, 1883. *B. Volcanol.*, **44**, 467–490.

Lavigne, F., Paris, R., Grancher, D., Wassmer, P., Brunstein, D., Vautier, F., Leone, F., Flohic, F., De Coster, B., Gunawan, T. and **Gomez, C.** (2009) Reconstruction of tsunami inland propagation on December 26, 2004 in Banda Aceh, Indonesia, through field investigations. *Pure Appl. Geoph.*, **166**, 259–281.

Lawton, T.F., Shipley, K.W., Aschoff, J.L., Giles, K.A. and **Vega, F.J.** (2005) Basinward transport of Chicxulub ejecta by tsunami-induced backflow, La Popa basin, northeastern Mexico, and its implications for distribution of impact-related deposits flanking the Gulf of Mexico. *Geology*, **33**, 81–84.

Le Roux, J.P. and **Vargas, G.** (2005) Hydraulic behavior of tsunami backflows: insights from their modern and ancient deposits. *Environ. Geol.*, **49**, 65–75.

Leckebusch, G.C., Koffi, B., Ulbrich, U., Pinto, J.G., Spangehl, T. and **Zacharias, S.** (2006) Analysis of frequency and intensity of European winter storm events from a multi-model perspective, at synoptic and regional scales. *Clim. Res.*, **31**, 59–74.

Leckie, D.A. and **Walker, R.G.** (1982) Storm- and tide-dominated shorelines in Cretaceous Moosebar-Lower Gates

interval outcrop equivalents of Deep Basin gas top in western Canada. *Bull. Am. Assoc. Petrol. Geol.*, **66**, 138–157.

Li, L., Qiu, Q. and **Huang, Z.** (2012) Numerical modeling of the morphological change in Lhok Nga, west Banda Aceh, during the 2004 Indian Ocean tsunami: understanding tsunami deposits using a forward modeling method. *Nat. Hazards*, **64**, 1549–1574.

Lorito, S., Tiberti, M.M., Basili, R., Piatanesi, A. and **Valensise, G.** (2008) Earthquake-generated tsunamis in the Mediterranean Sea: scenarios of potential threats to southern Italy. *J. Geophys. Res.-Sol. Ea.*, **113**, B01301.

MacDonald, R.G., Alexander, J., Bacon, J.C. and **Cooker, M.J.** (2009) Flow patterns, sedimentation and deposit architecture under a hydraulic jump on a non-eroding bed: defining hydraulic-jump unit bars. *Sedimentology*, **56**, 1346–1367.

MacInnes, B.T., Bourgeois, J., Pinegina, T.K. and **Kravchunovskaya, E.A.** (2009) Tsunami geomorphology: erosion and deposition from the 15 November 2006 Kuril Island tsunami. *Geology*, **37**, 995–998.

Mamo, B., Strotz, L. and **Dominey-Howes, D.** (2009) Tsunami sediments and their foraminiferal assemblages. *Earth-Sci. Rev.*, **96**, 263–278.

Maouche, S., Morhange, C. and **Meghraoui, M.** (2009) Large boulder accumulation on the Algerian coast evidence tsunami events in the western Mediterranean. *Mar. Geol.*, **262**, 96–104.

Marano, K.D., Wald, D.J. and **Allen, T.I.** (2010) Global earthquake casualties due to secondary effects: a quantitative analysis for improving rapid loss analyses. *Nat. Hazards*, **52**, 319–328.

Massari, F. (1996) Upper-flow-regime stratification types on steep-face, coarse-grained, Gilbert-type progradational wedges (Pleistocene, southern Italy). *J. Sed. Res.*, **66**, 364–375.

Massari, F. (2017) Supercritical-flow structures (backset-bedded sets and sediment waves) on high-gradient clinoform systems influenced by shallow-marine hydrodynamics. *Sed. Geol.*, **360**, 73–95.

Massari, F. and **D'Alessandro, A.** (2000) Tsunami-related scour-and-drape undulations in Middle Pliocene restricted-bay carbonate deposits (Salento, south Italy). *Sed. Geol.*, **135**, 265–281.

Massari, F., D'Alessandro, A. and **Davaud, E.** (2009) A coquinoid tsunamite from the Pliocene of Salento (SE Italy). *Sed. Geol.*, **221**, 7–18.

Masuda, F., Yokokawa, M. and **Sakamoto, T.** (1993) HCS mimics in Pleistocene, tidal deposits of the Shimosa Group and flood deposits of the Osaka Group, Japan. *J. Sed. Soc. Jpn.*, **39**, 27–34.

Matsui, T., Imamura, F., Tajika, E., Nakano, Y. and **Fujisawa, Y.** (2002) Generation and propagation of a tsunami from the Cretaceous-Tertiary impact event. In: *Catastrophic Events and Mass Extinctions, Impacts and Beyond* (Eds C. Koeberl and K.G. MacLeod), *Geol. S. Am. S.*, **356**, 69–77.

McMurtry, G.M., Watts, P., Fryer, G.J., Smith, J.R. and **Imamura, F.** (2004) Giant landslides, mega-tsunamis, and paleo-sea level in the Hawaiian Islands. *Mar. Geol.*, **203**, 219–233.

Minoura, K., Imamura, F., Sugawara, D., Kono, Y. and **Iwashita, T.** (2001) The 869 Jŏgan tsunami deposit and recurrence interval of large-scale tsunami on the Pacific coast of northeast Japan. *J. Nat. Disaster Sci.*, **23**, 83–88.

Monecke, K., Finger, W., Klarer, D., Kongko, W., McAdoo, B.G., Moore, A.L. and **Sudrajat, S.U.** (2008) A 1,000-year sediment record of tsunami recurrence in northern Sumatra. *Nature*, **455**, 1232–1234.

Moore, J.G. and **Moore, G.W.** (1988) Deposit from a giant wave on the island of Lanai, Hawaii. *Science*, **226**, 1312–1315.

Moore, A., Nishimura, Y., Gelfenbaum, G., Kamataki, T. and **Triyono, R.** (2006) Sedimentary deposits of the 26 December 2004 tsunami on the northwest coast of Aceh, Indonesia. *Earth Planet Space*, **58**, 253–258.

Morgan, O.W., Sribanditmongkol, P., Perera, C., Sulasmi, Y., Van Alphen, D. and **Sondorp, E.** (2006) Mass fatality management following the South Asian tsunami disaster: case studies in Thailand, Indonesia, and Sri Lanka. *PLoS Med.*, **3**, e195.

Morton, R.A., Gelfenbaum, G. and **Jaffe, B.E.** (2007) Physical criteria for distinguishing sand tsunami and storm deposits using modern examples. *Sed. Geol.*, **200**, 184–207.

Mulder, T., Razin, P. and **Faugeres, J.C.** (2009) Hummocky cross-stratification-like structures in deep-sea turbidites: Upper Cretaceous Basque basins (Western Pyrenees, France). *Sedimentology*, **56**, 997–1015.

Nanayama, F. and **Shigeno, K.** (2006) Inflow and outflow facies from the 1993 tsunami in southwest Hokkaido. *Sed. Geol.*, **187**, 139–158.

Nanayama, F., Shigeno, K., Satake, K., Shimokawa, K., Koitabashi, S., Miyasaka, S. and **Ishii, M.** (2000) Sedimentary differences between the 1993 Hokkaido-nansei-oki tsunami and the 1959 Miyakojima typhoon at Taisei, southwestern Hokkaido, northern Japan. *Sed. Geol.*, **135**, 255–264.

Nemec, W. (1990) Aspects of sediment movement on steep delta slopes. In: *Coarse-grained Deltas* (Eds A. Colella and D.B. Prior), *Int. Assoc. Sedimentol. Spec. Publ.*, **10**, 29–73.

Nigam, R. and **Chaturvedi, S.K.** (2006) Do inverted depositional sequences and allochthonous foraminifers in sediments along the Coast of Kachchh, NW India, indicate palaeostorm and/or tsunami effects? *Geo-Mar. Lett.*, **26**, 42–50.

Nissen, K.M., Leckebusch, G.C., Pinto, J.G., Renggli, D., Ulbrich, S. and **Ulbrich, U.** (2010) Cyclones causing wind storms in the Mediterranean: characteristics, trends and links to large-scale patterns. *Nat. Hazards Earth Sys.*, **10**, 1379–1391.

Okahashi, H., Akimoto, K., Mitamura, M., Hirose, K., Yasuhara, M. and **Yoshikawa, S.** (2002) Event deposits found in marsh sediments at Osatsu, Toba City, Mie Prefecture: identification of tsunami deposits using benthic foraminiferal fossils. *Chikyuu*, **24**, 698–703 (in Japanese).

Ono, K. and **Plink-Björklund, P.** (2017) Froude supercritical flow bedforms in deepwater slope channels? Field examples in conglomerates, sandstones and fine-grained deposits. *Sedimentology*. https://doi.org/10.1111/sed.12396.

Ontowirjo, B., Paris, R. and **Mano, A.** (2013) Modeling of coastal erosion and sediment deposition during the 2004 Indian Ocean tsunami in Lhok Nga, Sumatra, Indonesia. *Nat. Hazards*, **65**, 1967–1979.

Papadopoulos, G.A. and **Fokaefs, A.** (2005) Strong tsunamis in the Mediterranean Sea: a re-evaluation. *ISET J. Earthq. Technol.*, **42**, 159–170.

Paris, R., Fournier, J., Poizot, E., Etienne, S., Morin, J., Lavigne, F. and **Wassmer, P.** (2010) Boulder and fine sediment transport and deposition by the 2004 tsunami in Lhok Nga (western Banda Aceh, Sumatra, Indonesia): a coupled offshore–onshore model. *Mar. Geol.*, **268**, 43–54.

Pickering, K.T., Soh, W. and **Taira, A.** (1991) Scale of tsunami-generated sedimentary structures in deep water. *J. Geol. Soc. London*, **148**, 211–214.

Pomar, L., Obrador, A. and **Westphal, H.** (2002) Sub-wavebase cross-bedded grainstones on a distally steepened carbonate ramp, Upper Miocene, Menorca, Spain. *Sedimentology*, **49**, 139–169.

Postma, G., Roep, T.B. and **Ruegg, G.H.** (1983) Sandy-gravelly mass-flow deposits in an icemarginal lake (Saalian, Leuvenumsche Beek Valley, Veluwe, The Netherlands), with emphasis on plug-flow deposits. *Sed. Geol.*, **34**, 59–82.

Postma, G. and **Cartigny, M.J.B.** (2014) Supercritical and subcritical turbidity currents and their deposits—A synthesis. *Geology*, **42**, 987–990.

Postma, G., Cartigny, M.J.B. and **Kleverlaan, K.** (2009) Structureless, coarse-tail graded Bouma Ta formed by internal hydraulic jump of the turbidity current? *Sed. Geol.*, **219**, 1–6.

Postma, G., Kleverlaan, K. and **Cartigny, M.J.B.** (2014) Recognition of cyclic steps in sandy and gravelly turbidite sequences, and consequences for the Bouma facies model. *Sedimentology*, **61**, 2268–2290.

Pratt, B.R. (2002) Storms versus tsunamis: dynamic interplay of sedimentary, diagenetic, and tectonic processes in the Cambrian of Montana. *Geology*, **30**, 423–426.

Prendergast, A.L., Cupper, M.L., Jankaew, K. and **Sawai, Y.** (2012) Indian Ocean tsunami recurrence from optical dating of tsunami sand sheets in Thailand. *Mar. Geol.*, **295**, 20–27.

Pritchard, D. and **Dickinson, L.** (2008) Modelling the sedimentary signature of long waves on coasts: implications for tsunami reconstruction. *Sed. Geol.*, **206**, 42–57.

Puga-Bernabéu, Á. and **Aguirre, J.** (2017) Contrasting storm- versus tsunami-related shell beds in shallow-water ramps. *Palaeogeogr. Palaeocl.*, **471**, 1–14.

Puga-Bernabéu, Á., Martín, J.M. and **Braga, J.C.** (2007) Tsunami-related deposits in temperate carbonate ramps, Sorbas Basin, southern Spain. *Sed. Geol.*, **199**, 107–127.

Puga-Bernabéu, Á., Webster, J.M. and **Beaman, R.J.** (2013) Potential collapse of the upper slope and tsunami generation on the Great Barrier Reef margin, north-eastern Australia. *Nat. Hazards*, **66**, 557–575.

Puig, P., Ogston, A.S., Mullenbach, B.L., Nittrouer, C.A., Parsons, J.D. and **Sternberg, R.W.** (2004) Storm-induced sediment gravity flows at the head of the Eel submarine canyon, northern California margin. *J. Geophys. Res.-Oceans*, **109**, 128.

Ranasinghe, D.P., Goto, K., Takahashi, J., Wijetunge, J.J., Nishihata, T. and **Imamura, F.** (2013) Numerical assessment of bathymetric changes caused by the 2004 Indian Ocean tsunami at Kirinda fishery harbor, Sri Lanka. *Coast. Eng.*, **81**, 67–81.

Reimnitz, E. and **Marshall, N.F.** (1965) Effects of the Alaska earthquake and tsunami on recent deltaic sediments. *J. Geophys. Res.*, **70**, 2363–2376.

Rossetti, D.D.F., Góes, A.M., Truckenbrodt, W. and **Anaisse, J.** (2000) Tsunami-induced large-scale scour-and-fill structures in Late Albian to Cenomanian deposits of the Grajaú Basin, northern Brazil. *Sedimentology*, **47**, 309–323.

Rust, B.R. and **Gibling, M.R.** (1990) Three-dimensional antidunes as HCS mimics in a fluvial sandstone: the Pennsylvanian South Bar Formation near Sydney, Nova Scotia. *J. Sed. Res.*, **60**, 540–548.

Scheffers, A. and **Kelletat, D.** (2003) Sedimentologic and geomorphologic tsunami imprints worldwide—a review. *Earth-Sci. Rev.*, **63**, 83–92.

Schnyder, J., Baudin, F. and **Deconinck, J.F.** (2005) A possible tsunami deposit around the Jurassic-Cretaceous boundary in the Boulonnais area (northern France). *Sed. Geol.*, **177**, 209–227.

Shanmugam, G. (2006) The tsunamite problem. *J. Sed. Res.*, **76**, 718–730.

Shanmugam, G. (2012) Process-sedimentological challenges in distinguishing paleo-tsunami deposits. *Nat. Hazards*, **63**, 5–30.

Shiki, T. and **Yamazaki, T.** (1996) Tsunami-induced conglomerates in Miocene upper bathyal deposits, Chita Peninsula, central Japan. *Sed. Geol.*, **104**, 175–188.

Simons, D.B., Richardson, E.V. and **Nordin, C.F.** (1965) Sedimentary structures generated by flow in alluvial channels. In: *Primary Sedimentary Structures and Their Hydrodynamic Interpretation* (Ed G.V. Middleton), *SEPM Spec. Publ.*, **12**, 34–52.

Simpson, G. and **Castelltort, S.** (2006) Coupled model of surface water flow, sediment transport and morphological evolution. *Comput. Geosci.*, **32**, 1600–1614.

Slootman, A. (2016) *Supercritical Density Flow on Cool-Water Carbonate Ramps – The Lower Pleistocene of Favignana Island, Italy*. PhD Thesis University of Geneva, no. Sc. 5055. Retrieved from http://archive-ouverte.unige.ch/unige:92759

Slootman, A., Cartigny, M.J., Moscariello, A., Chiaradia, M. and **de Boer, P.L.** (2016) Quantification of tsunami-induced flows on a Mediterranean carbonate ramp reveals catastrophic evolution. *Earth Planet. Sci. Lett.*, **444**, 192–204.

Smit, J., Roep, Th. B., Alvarez, W., Montanari, A., Claeys, P., Grajales-Nishimura, J.M. and **Bermudez, J.** (1996) Coarse-grained, clastic sandstone complex at the K/T boundary around the Gulf of Mexico: deposition by tsunami waves induced by the Chicxulub impact? In: *The Cretaceous-Tertiary Event and Other Catastrophes in Earth History* (Eds G. Ryder, D. Fastovsky and S. Gartner), *Geol. S. Am. S.*, **307**, 151–182.

Soloviev, S.L., Solovieva, O.N., Go, C.N., Kim, K.S. and **Shchetnikov, N.A.** (2013) *Tsunamis in the Mediterranean Sea 2000 BC-2000 AD (Vol. 13)*. Springer Science & Business Media, Berlin, Germany.

Sørensen, M.B., Spada, M., Babeyko, A., Wiemer, S. and **Grünthal, G.** (2012) Probabilistic tsunami hazard in the Mediterranean Sea. *J. Geophys. Res.*, **117**, B01305.

Sugawara, D., Minoura, K. and **Imamura, F.** (2008) Tsunamis and tsunami sedimentology. In: *Tsunamiite* (Eds T. Shiki, Y. Tsuji, T. Yamazaki and K. Minoura), pp. 9–49. Elsevier B.V., Amsterdam, the Netherlands.

Sugawara, D., Goto, K. and **Jaffe, B.E.** (2014) Numerical models of tsunami sediment transport—current understanding and future directions. *Mar. Geol.*, **352**, 295–320.

Suppasri, A., Mas, E., Charvet, I., Gunasekera, R., Imai, K., Fukutani, Y., Abe, Y. and **Imamura, F.** (2013) Building damage characteristics based on surveyed data and fragility curves of the 2011 Great East Japan tsunami. *Nat. Hazards*, **66**, 319–341.

Takashimizu, Y. and **Masuda, F.** (2000) Depositional facies and sedimentary successions of earthquake-induced tsunami deposits in Upper Pleistocene incised valley fills, central Japan. *Sed. Geol.*, **135**, 231–239.

Tappin, D.R., Evans, H.M., Jordan, C.J., Richmond, B., Sugawara, D. and **Goto, K.** (2012) Coastal changes in the Sendai area from the impact of the 2011 Tōhoku-oki tsunami: interpretations of time series satellite images, helicopter-borne video footage and field observations. *Sed. Geol.*, **282**, 151–174.

Teh, S.Y., Koh, H.L., Liu, P.L.F., Ismail, A.I.M. and **Lee, H.L.** (2009) Analytical and numerical simulation of tsunami mitigation by mangroves in Penang, Malaysia. *J. Asian Earth Sci.*, **36**, 38–46.

Thuy, N.B., Tanaka, N. and **Tanimoto, K.** (2012) Tsunami mitigation by coastal vegetation considering the effect of tree breaking. *J. Coast. Conserv.*, **16**, 111–121.

Trigo, I.F., Davies, T.D. and **Bigg, G.R.** (1999) Objective climatology of cyclones in the Mediterranean region. *J. Climate*, **12**, 1685–1696.

Tsutsumi, A., Shimamoto, T., Kawamoto, E. and **Logan, J.M.** (2000) Nearshore flow velocity of Southwest-Hokkaido-Earthquake Tsunami. *J. Waterw. Port. C. Div.*, **126**, 136–143.

Tuttle, M.P., Ruffman, A., Anderson, T. and **Jeter, H.** (2004) Distinguishing tsunami from storm deposits in eastern North America: the 1929 Grand Banks tsunami versus the 1991 Halloween storm. *Seismol. Res. Lett.*, **75**, 117–131.

Uchida, J.I., Fujiwara, O., Hasegawa, S. and **Kamataki, T.** (2010) Sources and depositional processes of tsunami deposits: analysis using foraminiferal tests and hydrodynamic verification. *Isl. Arc.*, **19**, 427–442.

Umitsu, M., Tanavud, C. and **Patanakanog, B.** (2007) Effects of landforms on tsunami flow in the plains of Banda Aceh, Indonesia, and Nam Khem, Thailand. *Mar. Geol.*, **242**, 141–153.

Ward, S.N. (2001) Landslide tsunami. *J. Geophys. Res.-Sol. Ea.*, **106**, 11201–11215.

Ward, S.N. and **Asphaug, E.** (2000) Asteroid impact tsunami: a probabilistic hazard assessment. *Icarus*, **145**, 64–78.

Weiss, R. (2008) Sediment grains moved by passing tsunami waves: tsunami deposits in deep water. *Mar. Geol.*, **250**, 251–257.

Weiss, R. and **Bahlburg, H.** (2006) A note on the preservation of offshore tsunami deposits. *J. Sed. Res.*, **76**, 1267–1273.

Witter, R.C., Kelsey, H.M. and **Hemphill-Haley, E.** (2001) Pacific storms, El Nino and tsunamis: competing mechanisms for sand deposition in a coastal marsh, Euchre Creek, Oregon. *J. Coastal Res.*, **17**, 563–583.

Xiao, H., Young, Y.L. and **Prévost, J.H.** (2010) Hydro-and morpho-dynamic modeling of breaking solitary waves over a fine sand beach. Part II: numerical simulation. *Mar. Geol.*, **269**, 119–131.

Yamazaki, Y., Cheung, K.F. and **Kowalik, Z.** (2011) Depth-integrated, non-hydrostatic model with grid nesting for tsunami generation, propagation, and run-up. *Int. J. Numer. Meth. Fl.*, **67**, 2081–2107.

Yoshii, T., Tanaka, S. and **Matsuyama, M.** (2017) Tsunami deposits in a super-large wave flume. *Mar. Geol.*, **391**, 98–107.

Young, Y.L., Xiao, H. and **Maddux, T.** (2010) Hydro-and morpho-dynamic modeling of breaking solitary waves over a fine sand beach. Part I: experimental study. *Mar. Geol.*, **269**, 107–118.

Supporting Information

Additional Supporting Information may be found online in the supporting information tab for this article:

Data S1. A description of the numerical model of Simpson & Castelltort (2006) is available in the supporting information file.

